ORIGINAL CONTRIBUTION

# A facile approach to the fabrication of graphene-based nanocomposites by latex mixing and in situ reduction

Hui Li · Siduo Wu · Jinrong Wu · Guangsu Huang

**Abstract** Graphene-based polystyrene (PS) nanocomposites were prepared by latex mixing, co-coagulation, and in situ reduction process. In the process, aqueous dispersion of graphene oxide (GO) was mixed with PS latex, which was then co-coagulated with sodium chloride to form stabilized particle suspension; subsequently, hydrazine hydrate was added to reduce GO in situ. This process could avoid the use of additional surfactant or ultrasonic power to stabilize graphene during reduction, thus is facile and energy saving. The preparation process and the resulting nanocomposites were characterized in detail. The results show that, after co-coagulation, GO nanosheets are isolated by PS nanospheres through $\pi$–$\pi$ interaction, which prevents the restacking of graphene in the subsequent reduction process. Thus, a molecular-level dispersion of the graphene nanosheets in the PS matrix is achieved, which greatly improves the electrical conductivity and the mechanical properties of the nanocomposites.

**Keywords** Polystyrene · Graphene · Nanocomposite · Electric conductivity · Dynamic mechanics property

## Introduction

Graphene, a two-dimensional sheet composed of $sp^2$ carbon atoms, has attracted tremendous attention in recent years [1] because of its excellent electrical [2], thermal [3], and mechanical properties [4]. Thus, graphene is considered as an ideal multifunctional filler for polymers. There are

three main methods to incorporate graphene into polymer matrices, including in situ intercalative polymerization, solution blending, and melt blending [5]. The former two methods are effective in obtaining well-dispersed graphene nanosheets throughout the polymer matrix, which is crucial to harnessing various properties of graphene in polymer nanocomposites [6]. Although melt blending is the most economically attractive and scalable method, the greatest obstacle for its practical application is the self-aggregation of graphene nanosheets caused by strong van der Waals force, which is not easy to prevent [7].

Recently, a green method, i.e., latex technology, has been successfully developed to achieve good dispersion of graphene sheets in polymer matrices without using solvents. Generally, latex technology can be further subdivided into two categories: in situ emulsion polymerization and latex blending. Patole et al. [8] prepared graphene/polystyrene (G-PS) nanocomposites via in situ emulsion polymerization. In that work, sodium dodecyl sulfate-stabilized graphene nanosheets prepared by rapid thermal expansion of expandable graphite were mixed with styrene monomer and initiator, which were then polymerized to obtain nanocomposites with improved thermal stability and electrical conductivity. Hu et al. [9] directly mixed an aqueous dispersion of graphene oxide (GO) with styrene monomer, stabilizer, and initiator; after emulsion polymerization, hydrazine hydrate was added to reduce the GO nanosheets. However, their X-ray diffraction (XRD) measurement results indicated that there was significant restacking of graphene nanosheets in the G-PS nanocomposites. Another drawback for in situ emulsion polymerization is that graphene may have radical trapping capability [10], which leads to low conversion of monomer and low molecular weight of polymers.

Another strategy for latex technology is latex blending. However, a stable aqueous dispersion of graphene has to be

H. Li · S. Wu · J. Wu (✉) · G. Huang (✉)
College of Polymer Science and Engineering, State Key Laboratory of Polymer Materials Engineering, Sichuan University, Chengdu 610065, People's Republic of China
e-mail: wujinrong@scu.edu.cn
e-mail: guangsu-huang@hotmail.com

obtained firstly for the next blending process. One possible route is to chemically reduce GO in the presence of surfactant, for example, poly(sodium 4-styrenesulfonate) (PSS) [11]. Tkalya et al. [12] mixed an aqueous dispersion of PSS-stabilized graphene with polystyrene (PS) latex, which was subsequently freeze-dried and compressed to form G-PS nanocomposite with low percolation threshold. Nevertheless, the presence of foreign stabilizers is undesirable for the mechanical properties of polymers [13]. On the other hand, the surfactant may affect the conductivity of nanocomposites and reduce charge transport within the conductive network [14]. Another way for latex blending is to disperse GO in the polymer latex and then reduce GO to graphene that was stabilized with the aid of sonication [15]. However, sonication inevitably leads to degradation of polymers and is energy consuming; moreover, its large-scale preparation is limited.

In this study, we developed a facile approach based on latex blending without using additional stabilizer or sonication. In this approach, an aqueous dispersion of GO was firstly mixed with PS latex, then the mixture was subsequently co-coagulated with sodium chloride to form a suspension of particles in which GO nanosheets were isolated by PS nanospheres, and finally, hydrazine hydrate was added to reduce GO in situ. The obtained G-PS nanocomposites show not only high electrical conductivity but also improved mechanical properties.

## Experimental part

### Preparation of graphene oxide

GO was prepared via the oxidation of graphite (Hummers method [16]) and ultrasonication. The oxidation of graphite to graphite oxide was accomplished by treating graphite with a mixture of concentrated sulfuric acid, sodium nitrate, and potassium permanganate. The obtained graphite oxide was exfoliated by sonication for 2 h at 100 W to generate GO sheets.

### Preparation of polystyrene latex

PS latex was synthesized by conventional free radical emulsion polymerization. The process was described as follows: styrene monomer (100 ml), sodium dodecylbenzenesulfonate (SDBS, 3.62 g), and distilled water (500 ml) were mixed for 1 h, and then potassium persulfate (KPS, 0.45 g) was added dropwise. The reaction mixture was refluxed at 70 °C for 5 h under nitrogen atmosphere. Gel permeation chromatography analysis shows that the Mn, Mw, and PDI of the synthesized PS are 51 kg mol$^{-1}$, 179 kg mol$^{-1}$, and 3.5, respectively.

### Sample preparation

An appropriate amount of graphite oxide powders was redispersed in deionized water by sonication for 5 h to obtain the aqueous dispersion of GO. The dispersion process was monitored by the UV–Vis absorption spectra. The GO solution was mixed with PS latex. The mixture was then demulsified with saturated sodium chloride solution to obtain a suspension of particles which included both GO nanosheets and PS nanospheres. Subsequently, reduction reaction was carried out with hydrazine hydrate (1 ml for 20 mg GO) at 100 °C for 24 h under reflux. Afterwards, the mixture was cooled to room temperature and washed with deionized water to remove impurities. Finally, the purified product in the form of powder was dried in vacuum oven at 70 °C and then hot compressed to form sheets of 60×12×3 mm.

In order to investigate the degree of reduction of the powder samples with in situ reduction method, successive centrifugation/redissolution cycles [4] were employed to separate the graphene from the physically absorbed polymer. The centrifugation and dissolution procedure is described as follows: the composites (10 g) were dissolved in 100 ml N,N-dimethylformamide (DMF); the suspension was centrifuged at 10,000 rpm for 30 min to completely precipitate graphene. The obtained centrifugate was dissolved in the DMF again for 2 h, and then separated by centrifugation again. The resulting solid materials were washed extensively with methanol two times and dried at 70 °C under vacuum for 24 h.

### Characterization

Atomic force microscopy (AFM) images of GO were taken in the tapping mode by SPA400/SPI4000 (Seiko Instruments) with samples prepared by spin-coating the aqueous GO solutions onto the freshly cleaved mica substrates at 1,000 rpm. Transmission electron microscopy (TEM) observations were performed on a JEOL 2000/Hitachi H-7500 apparatus with an acceleration voltage of 80 kV. Ultrathin sections of the nanocomposites were prepared at ambient temperature using a Leica Ultracut UCT ultramicrotome with a diamond knife. XRD experiments were performed at room temperature with a X'Pert Pro MPD (Philips) diffractometer (Cu Kα radiation, X-ray wavelength 1.5406 Å). Raman spectra were recorded from 800 to 2,500 cm$^{-1}$ on a LABRAM HR800 confocal micro-Raman spectrometer using a 532-nm Nd:YAG laser. The X-ray photoelectron spectra (XPS) were performed with a Kratos XSAM800 instrument (Kratos Ltd., UK) using monochromatized Al Kα (1,486.6 eV) X-radiation. The electrical conductivities higher than $10^{-6}$ S/m were measured with a picoammeter (Keithley 6487) using a standard four-probe technique; the

electrical conductivities lower than $10^{-6}$ S/m were measured using a ZC36 high-resistance meter. The morphologies of PS nanospheres and the nanocomposite powders were investigated on an Inspect scanning electron microscopy (SEM) instrument (FEI) with an acceleration voltage of 20 kV. The dynamic mechanical analysis (TA Q800) was performed in dual cantilever mode with a frequency of 1 Hz in a temperature range from 25 to 160 °C.

## Results and discussion

Graphite oxide with layered structure can be readily exfoliated into single-layered GO in water by a gentle sonication process. Figure 1 shows the AFM image of GO after sonication. Most of the GO platelets exhibit a thickness below 1 nm, corresponding to one to two atomic layers.

The aqueous dispersion of GO was blended with PS latex by mechanical stirring for 30 min. Afterwards, the mixture was co-coagulated by saturated solution of sodium chloride, resulting in an aqueous suspension of micrometer-sized particles in which GO platelets were isolated by PS nanospheres. The SEM images of co-coagulated GO-PS particles are shown in Fig. 2. It is can be seen that the PS nanospheres are loosely stacked, making the micrometer-sized particles porous-like, which later allows the hydrazine



**Fig. 1** AFM analysis of GO sheets after sonication

hydrate molecules to penetrate through to reduce GO. The suspension of the particles remains stable for a few days.

GO is an amphiphile with hydrophilic edges and a more hydrophobic basal plane. Thus, GO can act the role of surfactant and be used to stabilize the polymer particles. As observed from the AFM images, the lateral size of GO is more than 1 μm, which is much larger than the PS nanospheres with diameters <100 nm (Fig. 3a). In the co-coagulation process, the SDBS molecules are pulled off from the surfaces of PS nanospheres, which makes the PS nanospheres be in direct contact with the GO nanosheets. Meanwhile, aromatic structures are known to interact strongly with the basal plane of the graphitic surface via π stacking [17]. Therefore, PS nanospheres can be anchored onto the surfaces of GO via π–π interaction, which is confirmed by the SEM observation in Fig. 3. Similar results were also reported by Hu et al. [9] and Zhao et al. [18].

To restore electrical conductivity, GO in the particles of the suspension is reduced with hydrazine hydrate; the extent to which GO has been reduced is analyzed by Raman spectroscopy. Raman spectroscopy has historically played an important role in the structural characterization of graphitic materials, in particular providing valuable information about defects and stacking of the graphene layers [19]. Figure 4 shows typical Raman spectra of GO and the G-PS nanocomposite with a graphene content of 10 wt%. It is clear that GO exhibits a strong band at 1,588 $cm^{-1}$ (G band) that corresponds to the first-order scattering of the $E_{2g}$ vibrational mode in the graphite sheet. In the spectra of the G-PS nanocomposite, a shift of the G band to higher frequency is observed, suggesting that the number of graphene layers is decreased [20, 21]. The D band at 1,350 $cm^{-1}$ of GO is associated with the structure defects of graphite. The intensity ratio ($I_D/I_G$) is increased from 0.89 for GO to 1.03 for G-PS nanocomposite, which is attributed to the formation some new and small $sp^2$ domains. The result suggests that the hydrazine molecules could penetrate the interstitial spaces between the PS particles to reduce the GO in the suspended particles, which leads to the formation of black G-PS composites. After reduction, the interaction between carbon atoms and the PS chain still exists and is enhanced. As illustrated in Fig. 3c, the PS particles are still adsorbed on the surface of chemical reduced graphene (RGO).

The dispersion of graphene nanosheets in the G-PS nanocomposites was detected by TEM and XRD measurements. Figure 5a shows the TEM images of the G-PS nanocomposite with 5 wt% loading of graphene. It is clear that the graphene nanosheets are finely dispersed in the PS matrix and aggregation is not found. During the procedure of oxidation and reduction, planar graphene carbons ($sp^2$-hybridized) were transformed into out-of-plane ones ($sp^3$-hybridized) by surface oxygen functionalities (C–O and C–O–C), resulting in the buckling of the sheets.
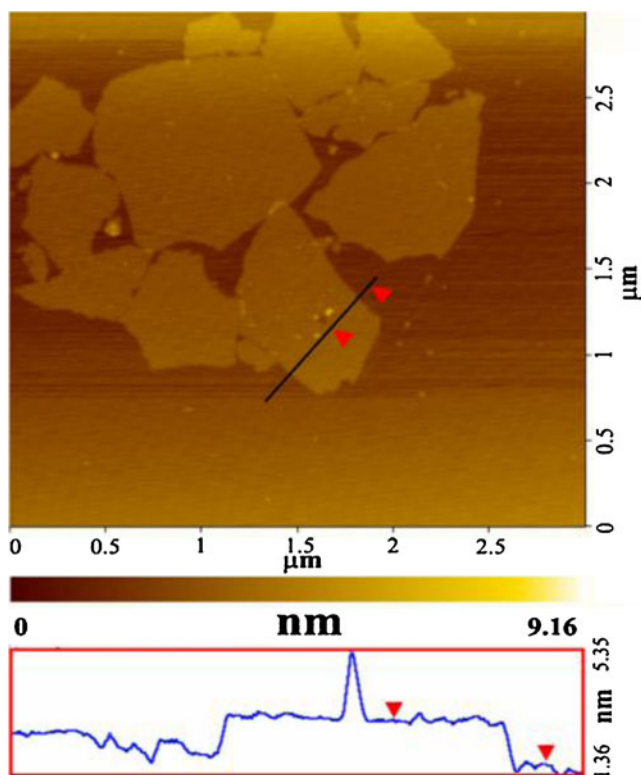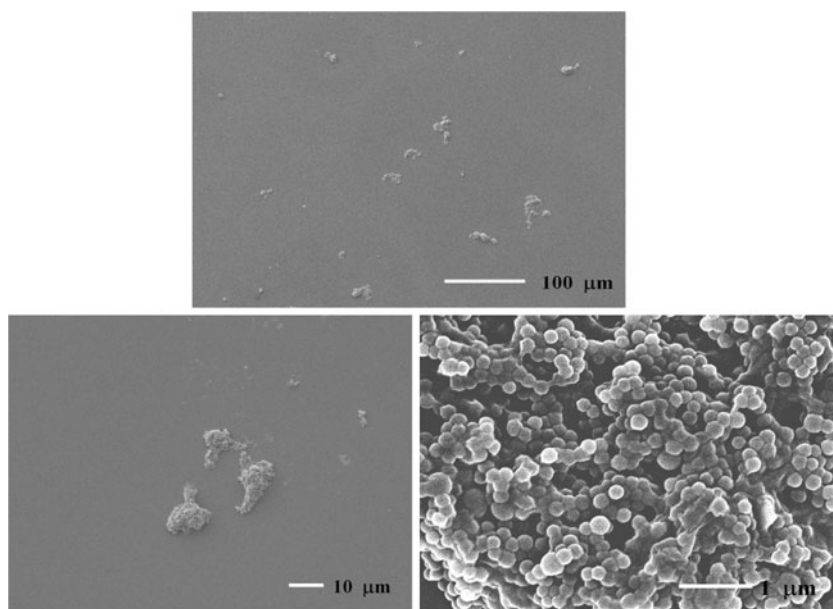
Fig. 2 SEM micrographs of
co-coagulated GO-PS particles
on a freshly exfoliated mica
substrate, dried down from a
highly diluted aqueous GO-PS
suspension



Therefore, chemically reduced graphene shows a wrinkled paper-like structure.

To further confirm the dispersion of graphene in the PS matrix, X-ray measurement was carried out for the G-PS nanocomposites, PS, GO, RGO and pristine graphite (Fig. 5b). The XRD patterns of the G-PS nanocomposites have the same broad $2\theta$ peak as that of pure PS at 19°, which is indicative of the intrinsic ordering of the amorphous polymer. Neither graphite layer structure peak at 26° corresponding to an interlayer spacing of 3.42 Å nor graphite oxide peak at 11° corresponding to $d_{spacing}$ of 8.03 Å was detected in the nanocomposites. Additionally, the RGO powders show a broad peak at 24.3° (interlayer spacing of 3.66 Å), presumably induced by the removal of the most of oxygen functional groups. However, a close inspection of the XRD patterns of G-PS composites reveals that there is no characteristic peak (or a slight shoulder peak) corresponding to the interlayer spacing of RGO. This result indicates that the dispersion of graphene nanosheets in the PS matrix is homogeneous and close to a single-sheet level [22].

To illustrate the advantages of our method, we also reduced GO before the co-coagulation process. The digital pictures of the G-PS composite prepared by the two different ways were recorded in Fig. 6. For the G-PS composite in which GO was reduced before co-coagulation, the graphene nanosheets could easily form a restacked structure due to the fact that PS nanospheres are not adsorbed onto their surfaces, thus could not form stable separation between the graphene nanosheets. As a result, a major part of the PS nanospheres are excluded from the restacked graphene nanosheets and still exists in the form of white PS latex (the lower part in Fig. 6a), while a small part of PS

nanospheres are bounded with the graphene nanosheets to form black G-PS suspension particles (the upper part in Fig. 6a). However, if GO was reduced after co-coagulation, all the PS nanospheres undergo an aggregation process and adsorbed onto the surfaces of GO, and they together formed micrometer-sized particle suspension. After reduction, the system demonstrates homogeneous black throughout the whole system because all of the particles contain graphene nanosheets (Fig. 6b). After setting aside for a few minutes, the composite becomes separated from the water. A significant difference can also be observed with respect to electrical conductivity. If the graphene content is 2 wt%, the electrical conductivity of the nanocomposite prepared by the former method is $2.0\times10^{-13}$ S/m, i.e., electrical isolating, indicating poor dispersion of graphene in the PS matrix. However, prepared by reducing GO after co-coagulation, the electrical conductivity of the nanocomposite is as high as $4.66\times10^{-4}$ S/m, suggesting that graphene is finely dispersed in the PS matrix to form electrical conductive paths.

Elemental analysis by XPS test was used to investigate the degree of reduction of graphene within the powder samples with two in situ reduction methods (the former way: GO was reduced after co-coagulation; the latter way: GO was reduced before co-coagulation). The C/O atomic ratio of graphite oxide is 3.3. The C/O ratio of the G-PS nanocomposites prepared by the former way is 9.9, while that for the G-PS nanocomposites prepared by the latter way is 6.4. The result shows that GO is reduced by reaction with hydrazine in the two in situ reduction methods; however, the degree of reduction within the latter way is lower than that of the former. Although there is difference of reduction efficiency between the two methods, the higher

**Fig. 3** SEM images to present the procedure to form G-PS nanocomposites with two different magnifications: **a** the pure PS particles, **b** GO-PS composite, **c** G-PS composite
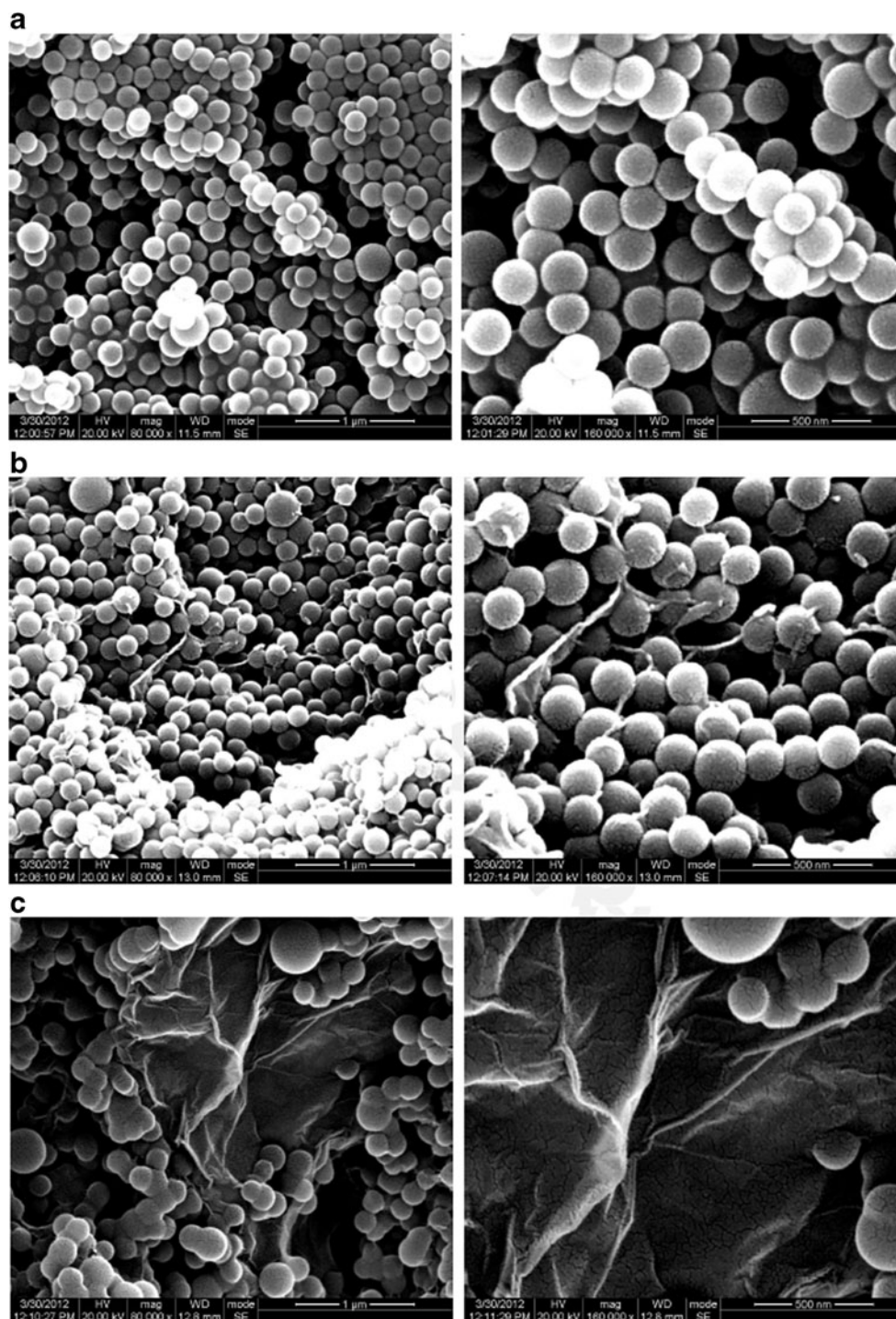


electrical conductivity of the nanocomposites prepared by the latter method is mainly attributed to the better dispersion of graphene and the formation of electrical conductive paths.

For clarity, the procedure to prepare G-PS nanocomposite is illustrated in Scheme 1. In the first step, the PS nanospheres which were formed by the SDBS coverage were mixed with the aqueous dispersion of GO. And then, the co-coagulation process was carrying out to provide anchoring effect between GO and PS nanospheres caused by the conjugation originating from the random contact of carbon atoms and PS chains. Finally, the PS microspheres-attached GO was reduced in situ with hydrazine hydrate to obtain G-PS nanocomposites. This procedure provides an attractive route to the large-scale production of graphene-based nanocomposites without the need of stabilizers or sonication.

Conductivity is a valuable qualitative measure of the conversion of GO to graphene. The electrical conductivity
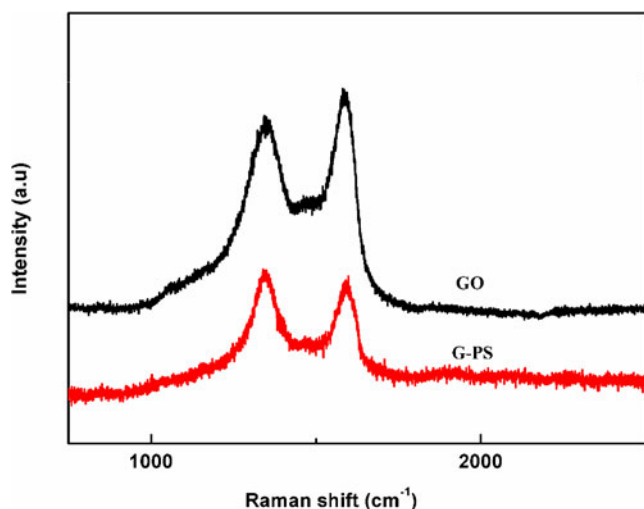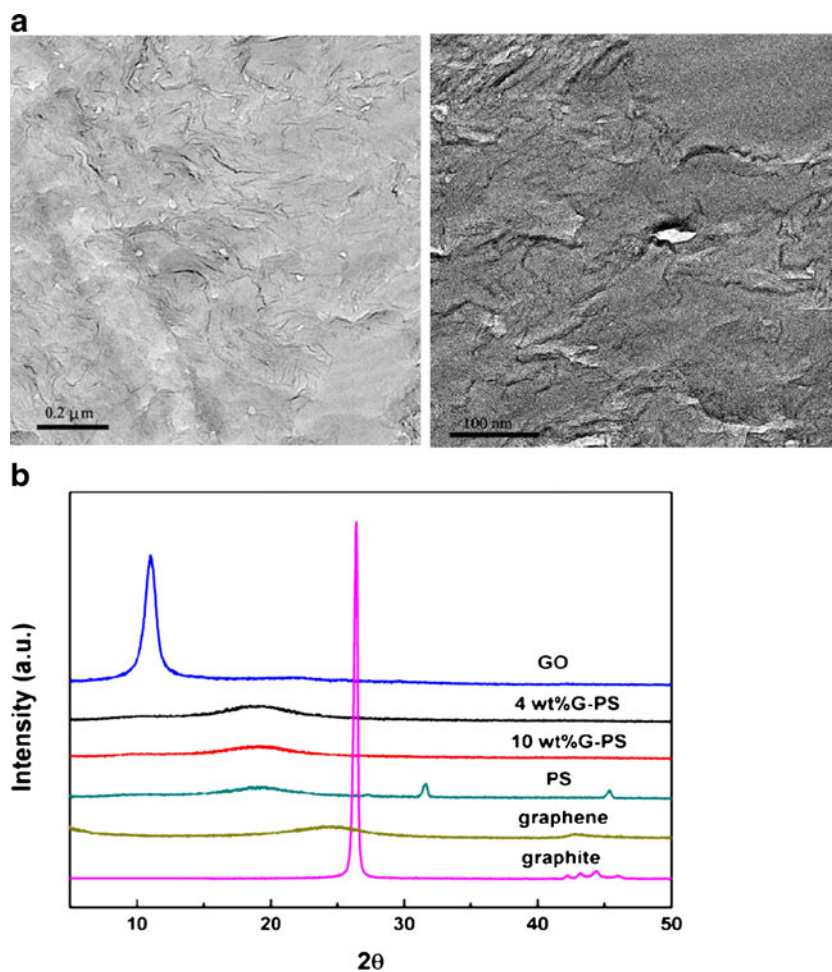
**Fig. 4** Raman spectroscopy of the GO and 10 wt% G-PS nanocomposite

of the G-PS nanocomposites as a function of the nanofiller content is shown in Fig. 7. It is evident that the electrical conductivity of the nanocomposites increases with the increase of the graphene content. When the graphene content

was about 1.5 wt%, the conductivity was only of the order of $10^{-7}$ S/m. At a loading of about 2 wt%, the conductivity of the nanocomposites has a distinct increase which already satisfies the antistatic criterion ($10^{-6}$ S/m), and thereafter, it rises rapidly, indicating that the conductive network structure has been successfully achieved. The composite with 8 wt% graphene possesses a conductivity of 2.55 S/m, which is sufficient for many electrical applications. The result also suggests the restoration of the conductive structure of graphene in the polymeric matrices.

The dispersed states of graphene also can be demonstrated by modulus changes of the composites. Figure 8 shows the variation of storage modulus as a function of temperature for pure PS and the nanocomposites with various graphene loadings. As illustrated in Fig. 8a, the storage modulus of the nanocomposites is higher than that of pure PS in the whole range of temperature and gradually increases with increasing graphene loading, which is attributed to the mechanical reinforcement effect of graphene. Meanwhile, the storage modulus of the nanocomposites at different temperatures shows distinctly different enhancement over that of the pure PS. At temperatures below the glass transition temperature ($T_g$) of

**Fig. 5 a** TEM images of G-PS nanocomposite with 5 wt% loading; **b** XRD of PS, GO, graphite, graphene and G-PS nanocomposites

**Fig. 6** Digital pictures of G-PS nanocomposites prepared by different ways at a graphene loading of 10 wt%: **a** GO was reduced before co-coagulation; **b** GO was reduced after co-coagulation; the *left panels* in **a** and **b** show that the reaction was finished completely, the *right panels* show the samples set aside for a few minutes
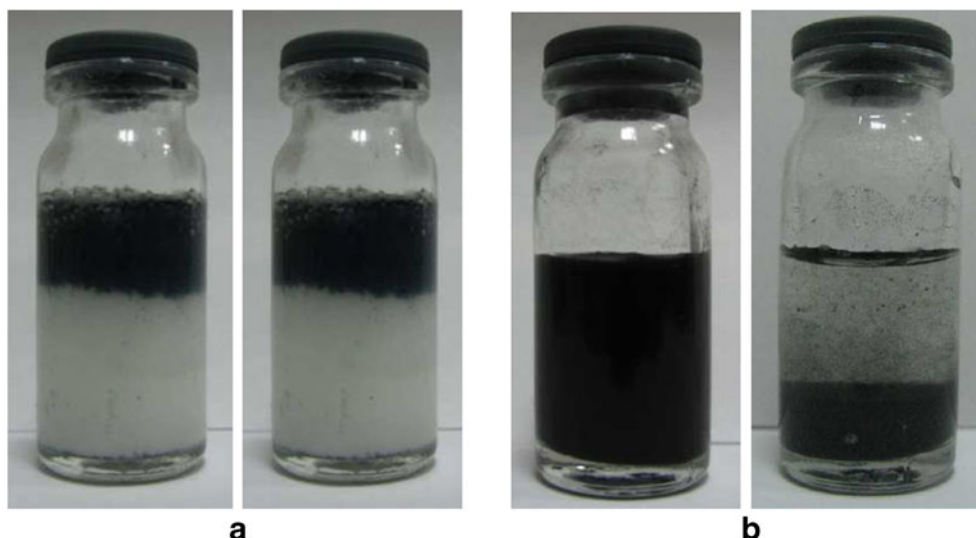
PS, the nanocomposites only show a slight increase in storage modulus as compared with the pure PS. With increasing temperature, the modulus suddenly drops by several orders of magnitude corresponding to the $T_g$ of the PS at about 100 °C. Above that temperature, the modulus of the nanocomposites is several times higher than that of pure PS in the rubbery state, suggesting that graphene is more efficient in improving the mechanical property of rubbery polymers, which was also found in some previous works [23].

To quantify the dispersion state of graphene in the nanocomposites in terms of an average aspect ratio, the experimental data are further compared with the theoretical predictions based on the rule of the Halpin–Tsai model which has been widely used to predict the modulus of composites filled with ellipsoidal fillers [13, 24–27]:

$$E = E_m \left[ \frac{3}{8} \frac{1 + \eta_L \xi V_c}{1 - \eta_L V_c} + \frac{5}{8} \frac{1 + 2\eta_T V_c}{1 - \eta_T V_c} \right] \qquad (1)$$

$$\eta_L = \frac{E_g/E_m - 1}{E_g/E_m + \xi} \qquad (2)$$

$$\eta_T = \frac{E_g/E_m - 1}{E_g/E_m + 2} \qquad (3)$$
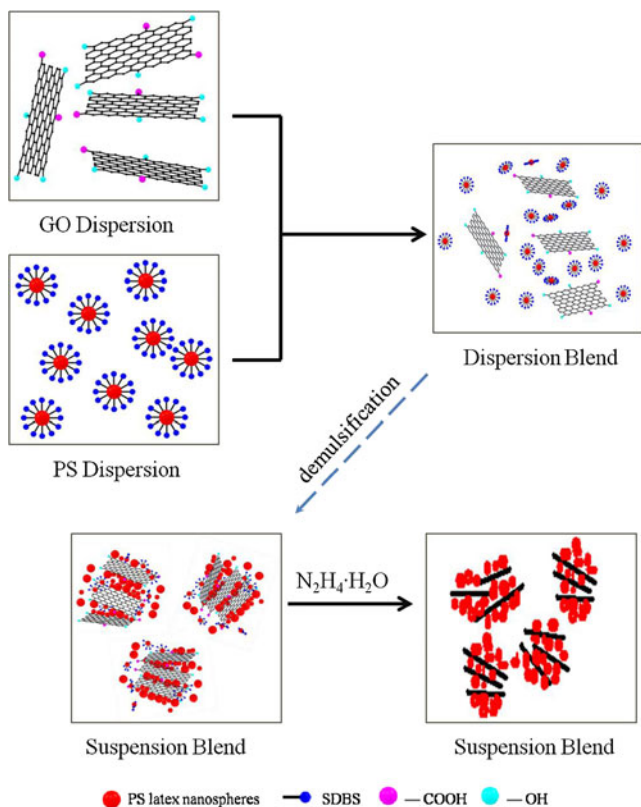


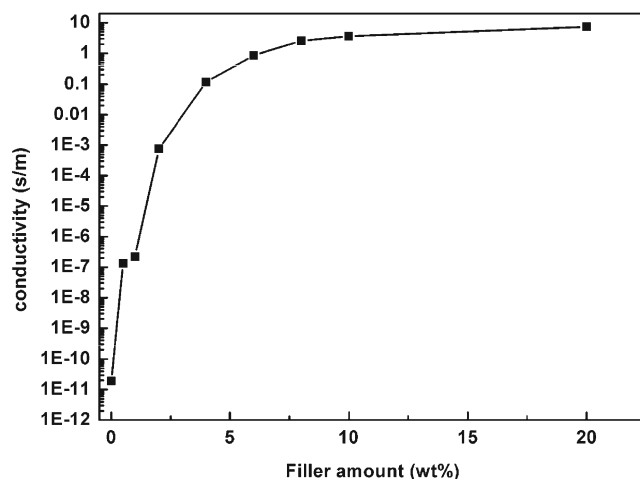**Scheme 1** Schematic of the formation procedure of G-PS nanocomposites



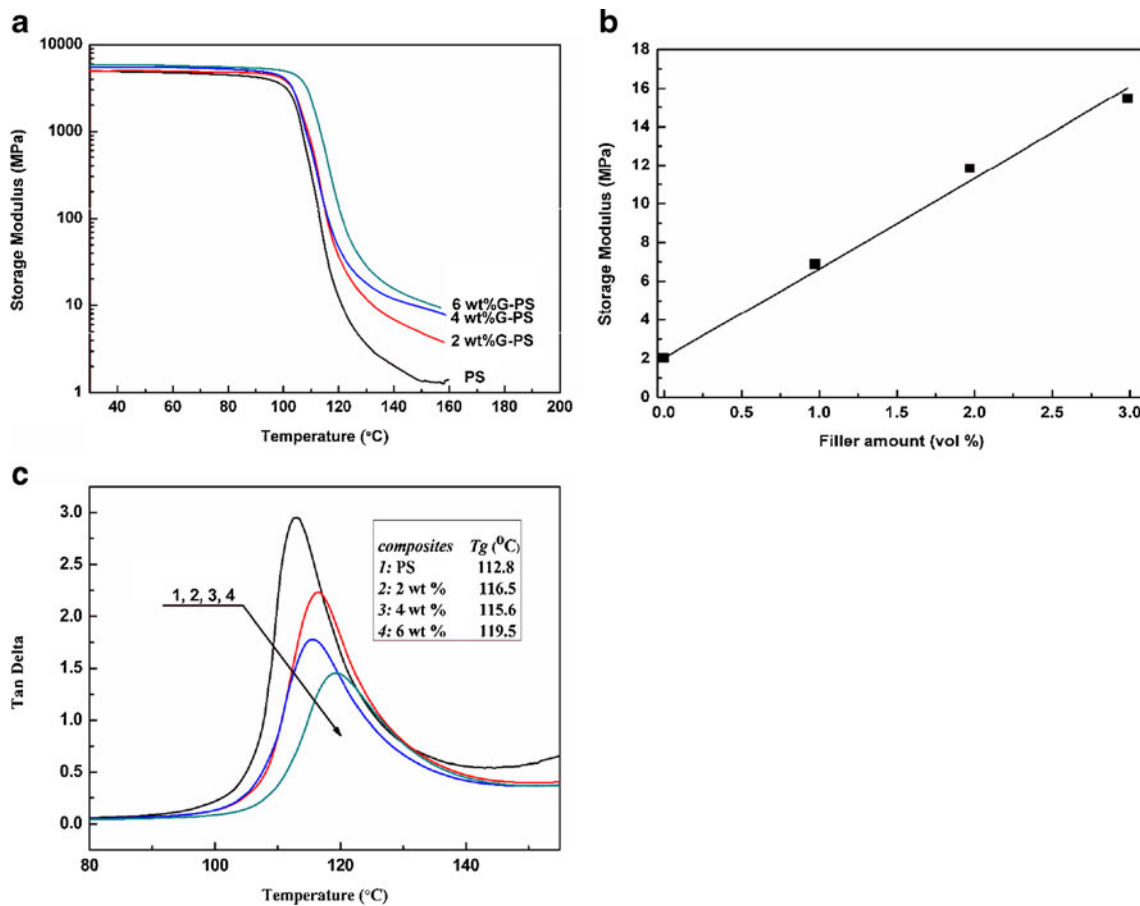**Fig. 7** Electrical conductivity of G-PS composites as a function of graphene weight fraction

**Fig. 8 a** Variation of the storage modulus of PS and G-PS composites as a function of the temperature; **b** storage modulus of PS and G-PS nanocomposites at 140 °C; **c** tanδ curves of PS and G-PS nanocomposites

$$\xi = 2\alpha_g/3 = 2l_g/3t_g \tag{4}$$

where $E_m$ and $E_g$ are the storage modulus of PS and graphene, respectively, and $\alpha_g$, $l_g$, and $t_g$ represent the aspect ratio, wideness, and thickness of the graphene sheets, respectively, and $V_c$ refers to the volume fraction of graphene in the nanocomposites. In the model, we allow $\xi$ to be a free-fitting parameter, so that the Halpin–Tsai model can best fit the modulus increase as a function of filler loading.

The modulus of graphene sheets derived from GO, as an important component of the Halpin–Tsai model, is usually determined to be 250 GPa [23, 28]. $E_m$ for PS was measured to be 2.038 MPa at 140 °C. It can be seen from Fig. 8b that the theoretical storage modulus of the nanocomposites is in good agreement with the test data using the Halpin–Tsai equation which gives a $\xi$ value of 591, thus the aspect ratio of graphene is 886.5, suggesting the molecular-level dispersion of graphene in the nanocomposites.

Figure 8c shows the tanδ curves for the G-PS nanocomposites as a function of graphene. It is evident that $T_g$ of the nanocomposites slightly shifts to higher temperature with increasing graphene loading, from 112.8 to 116.5,

115.6, and 119.5 °C with 2, 4, and 6 wt% of graphene loading, respectively, suggesting that the thermal stability of the nanocomposites is improved. In addition, the introduction of graphene results in a sharp decrease in the area under the damping peak, indicating that the segmental mobility of the PS chains during the glass transition is significantly limited and obstructed by the presence of graphene [23, 28, 29].

## Conclusion

The G-PS nanocomposites were prepared by latex mixing, co-coagulation, and reduction of GO with hydrazine hydrate. This procedure provides a simple path to the large-scale production of graphene-based nanocomposites without the need of stabilizers or sonication. SEM images show that the PS nanoparticles adsorb on the surface of graphene sheets by means of π stacking, especially along the basal planes of the graphene sheets. TEM and XRD measurements indicate that the graphene nanosheets can be well dispersed in PS as single-layer sheets. Therefore, the properties of the PS matrix are

significantly improved with the aid of graphene. The electrical conductivity of composite at a load of 8.0 wt% is 11 orders of magnitude higher than that of pure PS which is attributed to the formation of conductive network in the polymer matrix. In addition, the dynamic mechanical properties of the nanocomposites are greatly improved by the incorporation of graphene.

## References

1. Geim AK, Novoselov KS (2007) The rise of graphene. Nat Mater 6:183
2. Du X, Skachko I, Barker A, Andrei EY (2008) Approaching ballistic transport in suspended graphene. Nat Nanotechnol 3:491
3. Alexander A, Balandin, Suchismita G, Wenzhong B, Irene C, Desalegne T, Feng M, Lau CN (2008) Superior thermal conductivity of single-layer graphene. Nano Lett 8:902
4. Liu K, Chen L, Chen Y, Wu J, Zhang W, Chen F, Fu Q (2011) Preparation of polyester/reduced graphene oxide composites via in situ melt polycondensation and simultaneous thermo-reduction of graphene oxide. J Mater Chem 21:8612
5. Kim H, Abdala AA, Macosko CW (2010) Graphene/polymer nanocomposites. Macromolecules 43:6515
6. Kim H, Miura Y, Macosko CW (2010) Graphene/polyurethane nanocomposites for improved gas barrier and electrical conductivity. Chem Mater 22:3441
7. Li D, Müller MB, Gilje S, Kaner RB, Wallace GG (2008) Processable aqueous dispersions of graphene nanosheets. Nat Nanotechnol 3:101
8. Patole AS, Patole SP, Kang H, Yoo J-B, Kim T-H, Ahn J-H (2010) A facile approach to the fabrication of graphene/polystyrene nanocomposite by in situ microemulsion polymerization. J Colloid Interface Sci 350:530
9. Hu H, Wang X, Wang J, Wan L, Liu F, Zheng H, Chen R, Xu C (2010) Preparation and properties of graphene nanosheets–polystyrene nanocomposites via in situ emulsion polymerization. Chem Phys Lett 484:247
10. Fenoglio I, Tomatis M, Lison D, Muller J, Fonseca A, Nagy JB, Fubini B (2006) Reactivity of carbon nanotubes: free radical generation or scavenging activity? Free Radical Bio Med 40:1227
11. Stankovich S, Piner RD, Chen X, Wu N, Nguyen ST, Ruoff RS (2006) Stable aqueous dispersions of graphitic nanoplatelets via the reduction of exfoliated graphite oxide in the presence of poly(sodium 4-styrenesulfonate). J Mater Chem 16:155
12. Tkalya E, Ghislandi M, Alekseev A, Koning C, Loos J (2010) Latex-based concept for the preparation of graphene-based polymer nanocomposites. J Mater Chem 20:3035
13. Schaefer DW, Justice RS (2007) How nano are nanocomposites. Macromolecules 40:8501
14. Yu J, Lu K, Sourty E, Grossiord N, Koning CE, Loos J (2007) Characterization of conductive multiwall carbon nanotube/polystyrene composites prepared by latex technology. Carbon 45:2897
15. Zhan Y, Wu J, Xia H, Yan N, Fei G, Yuan G (2011) Dispersion and exfoliation of graphene in rubber by an ultrasonically-assisted latex mixing and in situ reduction process. Macromol Mater Eng 296:590
16. Hummers WS, Offeman RE (1958) Preparation of graphitic oxide. J Am Chem Soc 80:1339
17. Chen RJ, Zhang Y, Wang D, Dai H (2001) Noncovalent sidewall functionalization of single-walled carbon nanotubes for protein immobilization. J Am Chem Soc 123:3838
18. Song X, Yang Y, Liu J, Zhao H (2011) PS colloidal particles stabilized by graphene oxide. Langmuir 27:1186
19. Pimenta MA, Dresselhaus G, Dresselhaus MS, Cancado LG, Jorio A, Saito R (2007) Studying disorder in graphite-based systems by Raman spectroscopy. Phys Chem Chem Phys 9:1276
20. Shen J, Hu Y, Shi M, Lu X, Qin C, Li C, Ye M (2009) Fast and facile preparation of graphene oxide and reduced graphene oxide nanoplatelets. Chem Mater 21:3514
21. Rao CNR, Biswas K, Subrahmanyam KS, Govindaraj A (2009) Graphene, the new nanocarbon. J Mater Chem 19:2457
22. Ramanathan T, Abdala AA, Stankovich S, Dikin DA, Herrera-Alonso M, Piner RD, Adamson DH, Schniepp HC, Chen X, Ruoff RS, Nguyen ST, Aksay IA, Prud'Homme RK, Brinson LC (2008) Functionalized graphene sheets for polymer nanocomposites. Nat Nanotechnol 3:327
23. Pham VH, Cuong TV, Dang TT, Hur SH, Kong B-S, Kim EJ, Shin EW, Chung JS (2011) Superior conductive polystyrene—chemically converted graphene nanocomposite. J Mater Chem 21:11312
24. Xu J-Z, Chen T, Yang C-L, Li Z-M, Mao Y-M, Zeng B-Q, Hsiao BS (2010) Isothermal crystallization of poly(ʟ-lactide) induced by graphene nanosheets and carbon nanotubes: a comparative study. Macromolecules 43:5000
25. Nielsen LE (1970) Generalized equation for the elastic moduli of composite materials. J Appl Phys 41:4626
26. Tiwari RR, Khilar KC, Natarajan U (2008) New poly(phenylene oxide)/polystyrene blend nanocomposites with clay: intercalation, thermal and mechanical properties. J Appl Polym Sci 108:1818
27. Mark D, Frogley DR, Daniel Wagner H (2003) Mechanical properties of carbon nanoparticle-reinforced elastomers. Compos Sci Technol 63:1647
28. Potts JR, Lee SH, Alam TM, An J, Stoller MD, Piner RD, Ruoff RS (2011) Thermomechanical properties of chemically modified graphene/poly(methyl methacrylate) composites made by in situ polymerization. Carbon 49:2615
29. Vadukumpully S, Paul J, Mahanta N, Valiyaveettil S (2011) Flexible conductive graphene/poly(vinyl chloride) composite thin films with high mechanical strength and thermal stability. Carbon 49:198